The application of M12L24 nanocages as cell-specific siRNA delivery agents in vitro

Bobylev, E.O.; Zeng, Y.; Weijgertse, K.; Koelman, E.M.R.; Meijer, E.; Bruin, B. de; ... ; Reek, J.N.H.

Note: To cite this publication please use the final published version (if applicable).

Chem

Article

The application of M$_{12}$L$_{24}$ nanocages as cell-specific siRNA delivery agents *in vitro*
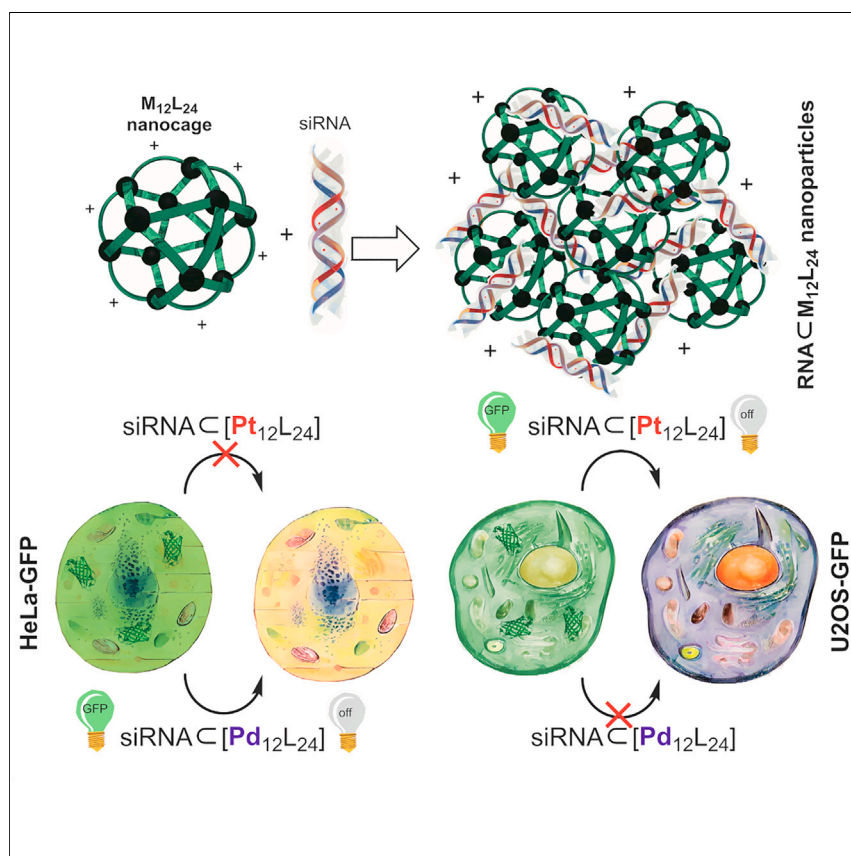
Reek and co-workers obtain nucleic-acid-binding M$_{12}$L$_{24}$ nanocages by utilizing building blocks with dual functionalities. The nanocages are functionalized with prominent nucleic acid binding sites. Whereas pyridinium and imidazolium nanocages are not effective in gene delivery, viologens Pd$_{12}$L$_{24}$ and Pt$_{12}$L$_{24}$ show cell-specific GFP silencing for the HeLa and U2OS cell lines, respectively. In contrast, the commercially applied vector (lipofectamine) does not differentiate between these cell lines in silencing experiments. This study presents M$_{12}$L$_{24}$ nanocages as a new class of siRNA vectors.

Eduard O. Bobylev, Ye Zeng, Kevin Weijgertse, ..., Bas de Bruin, Alexander Kros, Joost N.H. Reek

a.kros@chem.leidenuniv.nl (A.K.)
j.n.h.reek@uva.nl (J.N.H.R.)

Highlights

RNA delivery systems based on M$_{12}$L$_{24}$ nanocage-RNA composites are introduced

Tunable RNA binding strength and delivery efficiency

Cell-specific GFP silencing *in vitro* is achieved by changing the cage-forming metal

Specific GFP silencing by RRNA⊂Pd$_{12}$L$_{24}$ for HeLa cells and by RNA⊂Pt$_{12}$L$_{24}$ for U2OS cells

Article

The application of $M_{12}L_{24}$ nanocages as cell-specific siRNA delivery agents *in vitro*

Eduard O. Bobylev,[1,3] Ye Zeng,[2,3] Kevin Weijgertse,[2] Emma Koelman,[1] Eline M. Meijer,[1] Bas de Bruin,[1] Alexander Kros,[2,*] and Joost N.H. Reek[1,4,*]

SUMMARY

Small interfering RNA (siRNA) therapeutics have shown tremendous potential for the treatment of a range of diseases, but there is still a need for novel siRNA delivery materials. Here, we introduce $M_{12}L_{24}$ cages as siRNA delivery agents. We used four functionalized building blocks to form $M_{12}L_{24}$ nanocages. Dynamic light scattering showed that well-defined 130 nm nanocage/siRNA assemblies formed with positive zeta potentials. Cell-specific siRNA-mediated green fluorescent protein (GFP) silencing, controlled by the metal used for nanocage formation, was obtained. A $Pt_{12}L_{24}$ nanocage was highly effective in delivering siRNA to U2OS cells but showed little efficiency for HeLa cells. The less stable $Pd_{12}L_{24}$ nanocage derived from the same building block displayed effective GFP silencing for HeLa cells but not for U2OS cells. The ease of preparation and the ability to tune the binding strength, together with the specific siRNA delivery efficiency depending on the building blocks and metals, show potential for future siRNA delivery applications.

INTRODUCTION

In gene therapy, genetic material is used to regulate the expression of proteins, enzymes, and other targets or to modify the biological properties of cells for therapeutic requirements.[1–10] In past years, nucleic acids attracted increasing attention as a result of discoveries such as CRISPR genome editing[11,12] and RNA interference.[13–15] RNA-based therapeutics can manipulate gene expression (RNA interference) or produce therapeutic proteins, making them suitable for the treatment of pathological conditions ranging from infectious diseases, metabolic disorders, neurological diseases, and cancers to genetic disorders, including those that are considered "undruggable" with small molecules or monoclonal antibodies.[1–10,16] Small interfering RNA (siRNA; one type of therapeutically active RNA) is a double-stranded oligonucleotide consisting of 19–25 base pairs. It binds to the RNA-induced silencing complex (RISC) guides the cleavage of a targeted mRNA sequence to induce sequence-specific gene expression suppression (silencing).[17,18] In 2018, the FDA approved the first-ever siRNA therapeutic, called ONPATTRO (patisiran), which uses lipid nanoparticles (NPs) to deliver siRNA against mutant and wild-type transthyretin for the treatment of transthyretin-mediated amyloidosis.[19]

Therapeutic treatment using RNA is typically complementary to the application of conventional drugs (*vide supra*).[1,20–23] However, RNA molecules are negatively charged and hydrophilic and possess high molecular weight. Because of these properties, RNA molecules permeate cell membranes poorly, clear quickly from the extracellular matrix, and degrade easily.[24–26] Therefore, molecules that allow the

THE BIGGER PICTURE

RNA interference is gaining increasing attention for the treatment of various human diseases. Delivery agents (vectors) play a crucial role in introducing therapeutically active RNA into cells to regulate protein expression. Different types of non-viral vectors (such as dendrimers and liposomes) have been developed. However, some hurdles—such as a lack of selectivity, severe toxicity, and poor stability of formulations— still need to be overcome to pave the way for the future gene-medicinal field. In this study, we introduce $M_{12}L_{24}$ nanocages as a new class for RNA delivery. *In vitro* models with two different cell lines display selective siRNA delivery efficiency depending on the nanocage composition. With their versatile functionalization possibilities, size, charge, and structural integrity, $M_{12}L_{24}$ nanocages provide a valuable addition to the family of siRNA delivery vectors. The potential of these systems will need to be further explored and developed.
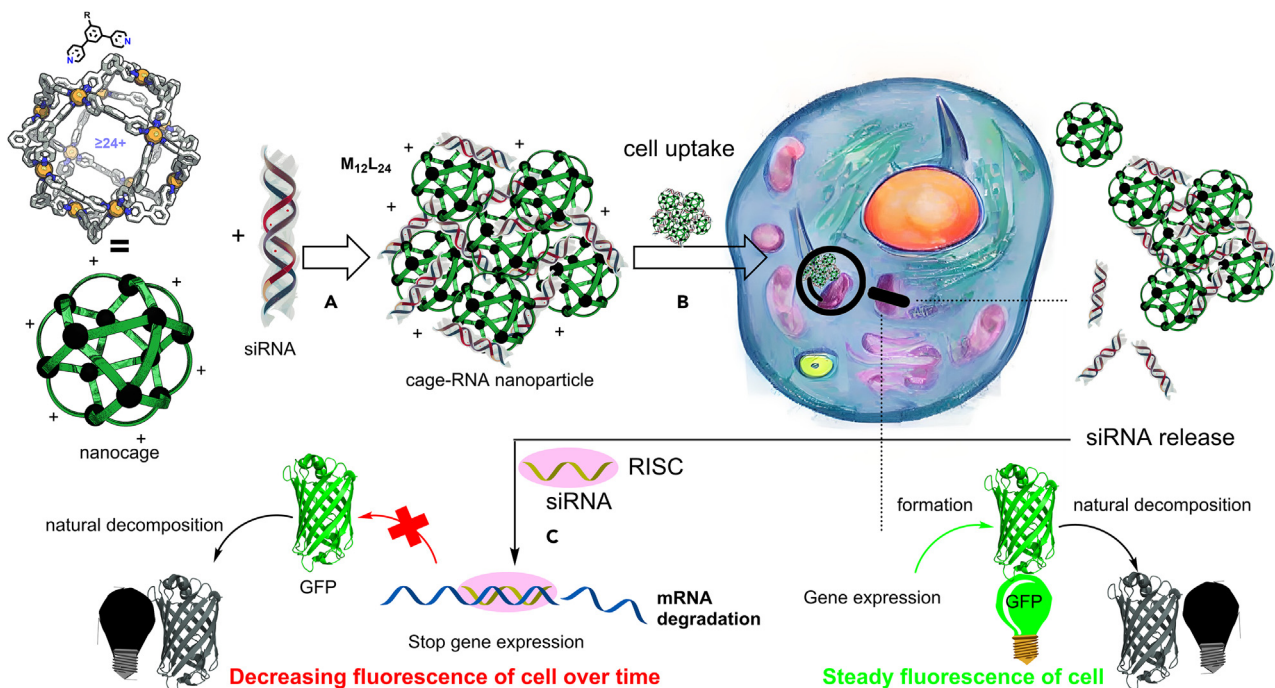
Figure 1. Schematic representation of the gene delivery assay of M$_{12}$L$_{24}$ nanocages (green; scheme applies to M = Pt^{2+}) on GFP-expressing cells

permeation of RNA through the cell membrane and protect gene material from degradation have been developed in the past decades. These RNA nanodelivery systems are called vectors. The currently most used non-viral vectors can be divided into different functional material groups, such as dendrimers,[27,28] lipid NPs,[29,30] liposomes,[31,32] metal-organic frameworks,[2,33–36] and polymers.[37,38] They have shown success in delivering RNA therapeutics, yet the fast-growing field of gene therapy[39,40] still requires novel vectors with high delivery efficiencies and high cell specificity.

Coordination-based spherical assemblies (CBSAs) have recently gained attention in the medicinal context.[41–44] CBSAs are well-defined nanosized materials that are constructed by coordination of multi-topic ligands to transition metals.[45–48] Some CBSAs have shown interesting properties regarding DNA/RNA binding because of their cationic charge and aromatic exterior. Examples include Ru$_3$L$^A_2$L$^B_3$ prisms,[49] octahedron Pt$_6$L$_4$,[50] tetrahedral Ni$_4$L$_6$,[51] helicate Ni$_2$L$_3$,[52] and cuboctahedral Pd$_{12}$L$_{24}$.[53] Whereas some studies have suggested the application of CBSAs as genotoxic agents, to the best of our knowledge their potential as gene delivery agents has never been investigated.

Inspired by the promising DNA-CBSA interactions reported in the literature, we have designed and studied gene delivery systems based on supramolecular nanocages *in vitro*. To do this, we used M$_{12}$L$_{24}$ cages[46,54–58] because these types of nanocages, with their large size, high charge, and structural and compositional stability, combine all requirements desired for good RNA vectors. We then studied the formation and properties of RNA⊂M$_{12}$L$_{24}$ NPs (Figure 1A), cell uptake (Figure 1B), and *in vitro* green fluorescence protein (GFP) silencing (Figure 1C). Finally, we show the ability of M$_{12}$L$_{24}$ cages to bind siRNA and cell-specific GFP silencing. This work presents M$_{12}$L$_{24}$ as a new class of siRNA vectors of which the stability can be

[1]van 't Hoff Institute for Molecular Sciences, University of Amsterdam, Science Park 904, 1098 XH Amsterdam, the Netherlands
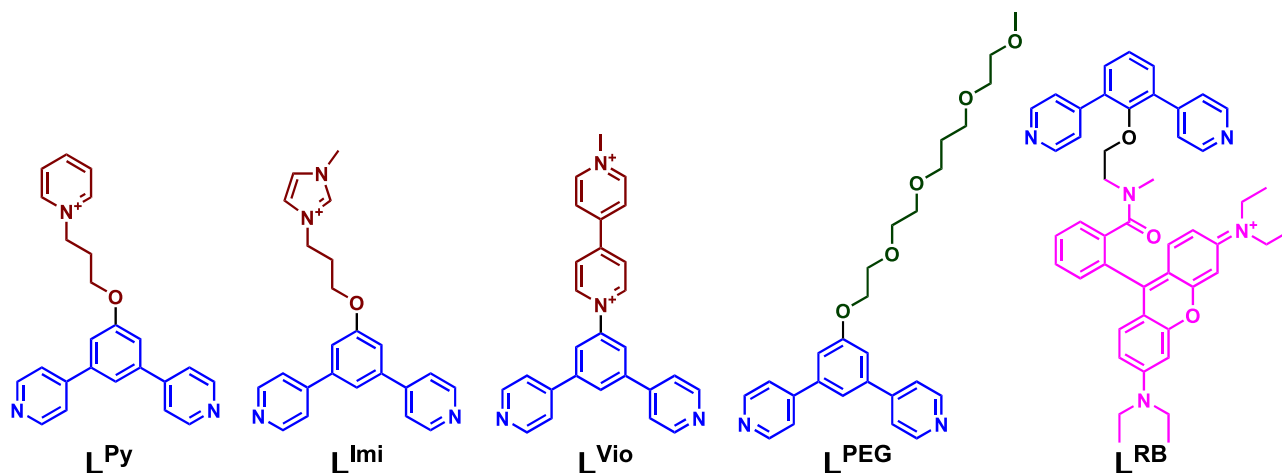
[2]Department of Supramolecular & Biomaterials Chemistry, Leiden Institute of Chemistry, Leiden University, P.O. Box 9502, 2300 RA, Leiden, the Netherlands

[3]These authors contributed equally

[4]Lead contact

*Correspondence:
a.kros@chem.leidenuniv.nl (A.K.),
j.n.h.reek@uva.nl (J.N.H.R.)

Figure 2. Chemical structure of the building blocks with dual function
Cage-forming site in blue, nucleic acid binding sites in red, fluorescent tag (rhodamine B) in pink.

tuned and the functionality can be easily modified, and with their unique size, they have the potential for future applications as vectors.

RESULTS AND DISCUSSION

Synthesis of nanocages

Four different building blocks with dual functionalities, a site for cage formation, and an RNA binding site were synthesized. All building blocks were prepared according to standard organic synthesis protocols (summarized in supplemental information section "synthesis of building blocks"). The set contained one neutral building block (L^{PEG}), two mono-cationic building blocks (L^{Py} and L^{Imi}), a double cationic building block (L^{Vio}), and a rhodamine-labeled building block (L^{RB}) (Figure 2).

$Pt_{12}L_{24}$ cages were prepared as previously described.[55] L^{Py} (1 equiv), $[Pt(BF_4)(MeCN)_4]$ (0.6 equiv), and a catalytic amount of TBACl (7 mol %) in acetonitrile-d_3 were heated at 150°C for 3 days (Figure 3A). A sharp ^{1}H-NMR spectrum was obtained, indicating the formation of a highly symmetrical structure (Figure 3C). The observed downfield shift of the pyridine protons was in line with coordination to platinum ($\Delta\delta(H^a) = +0.49$ ppm and $\Delta\delta(H^b) = +0.32$ ppm, Figure 3C). DOSY showed the appearance of a slower diffusing species (log D = -9.65 m$^2\cdot$s^{-1} for $[Pt_{12}(L^{Py})_{24}(BF_4)_{48}]$ compared with -8.89 m$^2\cdot$s^{-1} for the building block L^{Py}) with a calculated hydrodynamic radius of 2.8 nm, in line with the formation of the $Pt_{12}L_{24}$ nanocage (Figure 3B). Mass analysis by electrospray ionization high-resolution mass spectrometry (ESI-HR-MS) confirmed the selective formation of the desired structure by showing only signals corresponding to different charged states of the cage with the general formula $[Pt_{12}L^{Py}_{24}(BF_4)_x]^{(48-x)+}$ with a matching isotope pattern for x = 6–16 (Figure 3D). For all other building blocks, we applied the same experimental procedure as for the synthesis of $[Pt_{12}L^{Py}_{24}]$, which yielded the corresponding platinum cages with characteristic spectroscopic features similar to those of $[Pt_{12}L^{Py}_{24}]$ (supplemental information section "nanocage synthesis"). Next to the platinum-based nanocages, one palladium cage, $[Pd_{12}L^{Vio}_{24}]$, was prepared by a standard procedure.[54] All cages were obtained with excellent selectivity, as shown by ^{1}H-NMR and ESI-MS analysis. The cages were obtained as 0.42 mM solutions in acetonitrile-d_3. No further purification was required for the application in RNA binding. For simplification, we abbreviate the nanocages as **Pt(Vio)**, **Pt(Imi)**, **Pt(Py)**, and **Pd(Vio)** (Figure 4).
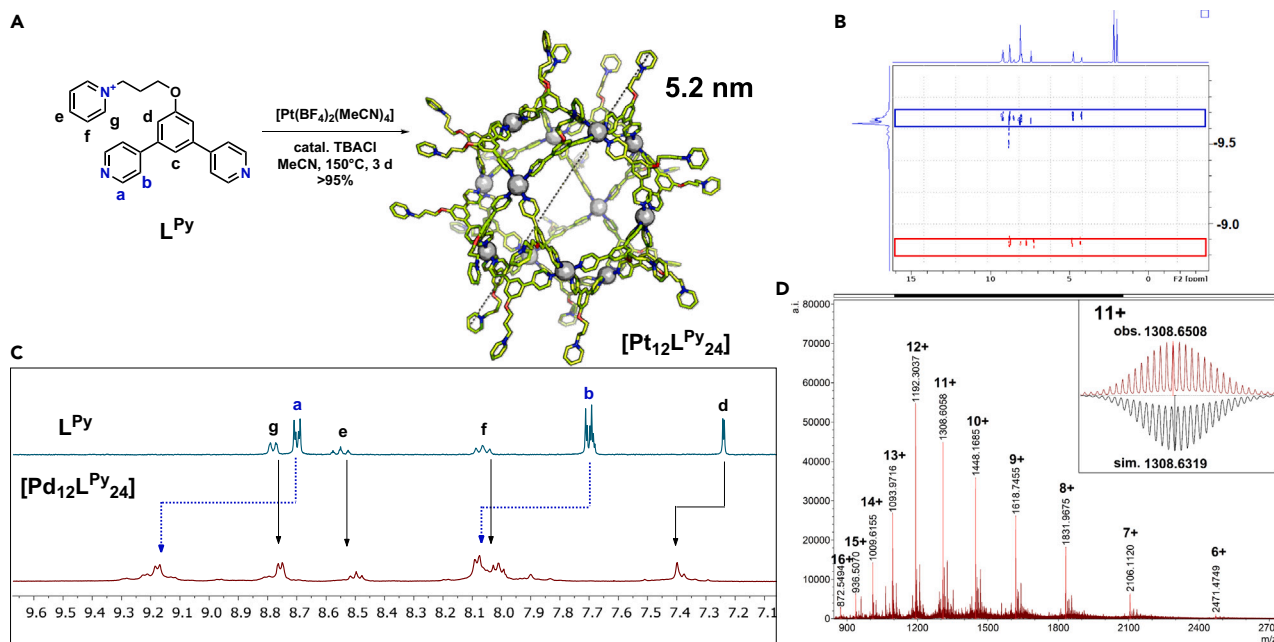
Figure 3. Synthesis and characterization of [Pt$_{12}$L$^{Py}_{24}$]$^{48+}$

(A) Reaction conditions for the formation of nanocages. The molecular structure of the displayed cage was minimized on the PM3 level. Carbon, yellow; nitrogen, blue; palladium, white cages.

(B) Overlaid DOSY NMR of the [Pt$_{12}$L$^{Py}_{24}$] cage (blue) and the building block (red).

(C) ^{1}H-NMR spectra of [Pt$_{12}$L$^{Py}_{24}$] cage and the corresponding building block.

(D) ESI-MS spectrum of [Pt$_{12}$L$^{Py}_{24}$].

Cage stability

The well-defined structure of M$_{12}$L$_{24}$ nanocages is expected to bind RNA. The integrity of the nanocages during the preparation of RNA⊂M$_{12}$L$_{24}$ NPs plays an important role. When unstable nanocages are used, it cannot be excluded that other materials (e.g., decomposition oligomers) are responsible for RNA complexation, and this would hamper any investigation into the rational design of the NP-forming structures.

We evaluated the stability of the various nanocages by using their unique UV-visible (UV-vis) absorbance. UV-vis absorbance spectra of all five cages (Figure 4) were measured at 37°C in acetonitrile, water, and phosphate-buffered saline (PBS, 1 M, pH 7.4) (Figures S33–S38). All nanocage absorbances were ~20 nm red-shifted in comparison with the corresponding building blocks as a result of the coordination to platinum/palladium (Figure S38). For Pt$_{12}$L$_{24}$ nanocages with L = L^{Py}, L^{Imi}, and L^{Vio}, absorption spectra showed no changes after 14 h at 37°C in PBS (Figures S33–S35), indicating that the cages are stable in the presence of halide and buffer. A decrease in absorbance was observed for **Pt(PEG)** and the palladium cage **Pd(Vio)** (Figures S36 and S37). Because **Pt(PEG)** and **Pd(Vio)** showed decreased absorption in PBS, we studied their stability in HEPES-buffered water (Figures S36 and S37). In HEPES-buffered water, no significant changes in the absorption of **Pt(PEG)** and **Pd(Vio)** were observed, supporting their stability in buffered water. Given that all nanocages are sufficiently stable in HEPES, HEPES-buffered water was used for the studies involving the preparation and characterization of RNA⊂M$_{12}$L$_{24}$ NPs.

Initial RNA binding assay

With Pt$_{12}$L$_{24}$ nanocages bearing different RNA binding sites on the exterior in hand, we performed initial binding studies to ^{AR}siRNA. For qualitative analysis of the binding, we
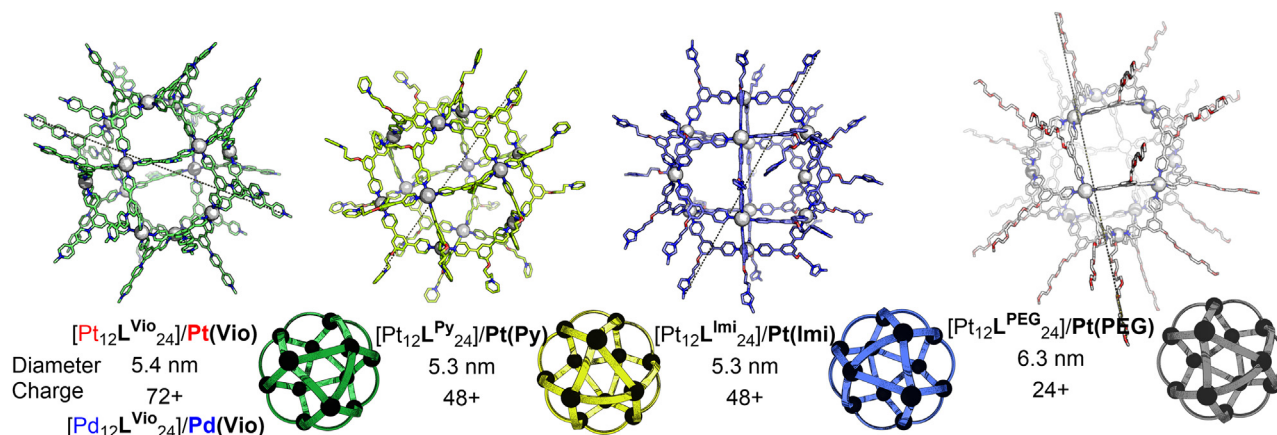
Figure 4. PM3-optimized structure of the four nanocages

used circular dichroism (CD) titrations to study the chiral nature of the nanocage and siRNA complex (Figure 5A). All binding studies were performed at room temperature in HEPES-buffered water (100 mM, pH 7.4), and nanocages were used as synthesized in acetonitrile-d$_3$. For all nanocage titrations, a decrease in ellipticity at λ = 265 nm and an increase in ellipticity at λ = 314 nm were observed (Figure 5B; these were attributed to absorptions of RNA and nanocages: Figure 5C), indicative of successful ^{AR}siRNA binding (Figure 5B; see supplemental information section "CD spectra" for further details). Given that both the nanocages and the ^{AR}siRNA represent multi-topic binders, an accurate binding constant could not be obtained from this set of experiments because the exact stoichiometry is unknown. For the relative comparison of the four nanocage-siRNA complexes, we approximated binding affinities on the basis of the relative decrease and increase in the CD ellipticity (by treating the RNA as a mono-binding unit and the nanocage as 24 identical units in a 1:1 ratio by using BindFit[59–61]). Following these simplified approximations, we obtained the highest affinity between **Pt(Vio)** and RNA (K$_a$ ≈ 1.1 ± 0.2 × 10^7 M$^{−1}$), followed by **Pt(Py)** ≈ **Pt(Imi)** (K$_a$ ≈ 4.5–5.8 ± 0.7 × 10^6 M$^{−1}$) and **Pt(PEG)** (K$_a$ ≈ 1.8 ± 0.2 × 10^6 M$^{−1}$) (Figure 5D), similar to the expected trend based on the individual charge and monomeric binding affinities. This indicates different binding affinities of the four nanocages with RNA, which allows for the formulation of nanocage-siRNA complexes.

Preparation of nanocage-siRNA NPs and characterization

After obtaining promising binding results between siRNA and the M$_{12}$L$_{24}$ nanocages, we investigated the formation of RNA⊂M$_{12}$L$_{24}$ NPs to support that nanocages are capable of forming stable NPs. Therefore, we formulated the NPs of the nanocages complexed with siRNA and evaluated the so-formed NPs' properties and their stability by dynamic light scattering (DLS) and gel electrophoresis.

We screened NP preparation using different P/N (positive charge/negative charge) ratios of nanocage to siRNA, from 1/1 to 32/1 (Table S6). All formulations resulted in the formation of well-defined NPs (a P/N ratio of 32 is discussed in the main text; for all ratios, see supplemental information sections "DLS and zeta potential of RNA⊂cage nanoparticles," "toxicity of RNA⊂cage nanoparticles," and "GFP silencing of RNA⊂cage nanoparticles"). The obtained NPs exhibited different hydrodynamic sizes with a narrow polydispersity index (PDI), ranging from 110 to 190 nm depending on the nanocage and stoichiometry (Figure 6A). The NPs remained stable for 14 days after preparation (Figure S58).
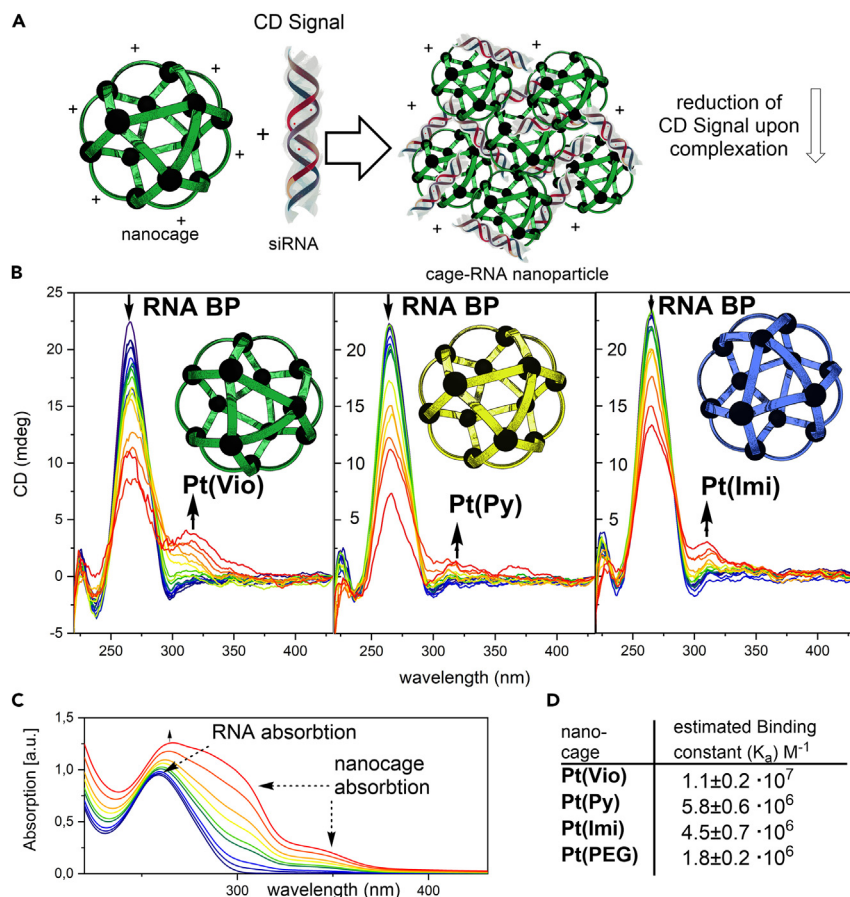
Figure 5. CD studies on RNA complexation with nanocages
(A) Schematic depiction of the performed experiments.
(B) Decrease in characteristic CD band associated with siRNA upon the addition of increasing amounts of nanocages as a result of complexation.
(C) UV-vis absorption over the course of a titration of **Pt(Py)** to siRNA and identification of the absorption bands.
(D) Estimated binding constants between nanocages and siRNA.

All NPs displayed a highly cationic surface charge, which is required for efficient cell uptake through negatively charged cell membranes (Figure 6A). Furthermore, quantitative encapsulation of siRNA within the NPs was proven by RNA agarose gel electrophoresis, given that no free siRNA was observed (Figures 6B and S59).

NPs composed of **Pt(Vio)**, **Pd(Vio)**, **Pt(Imi)**, **Pt(Py)**, **Pt(PEG)**, and siRNA (P/N ratio = 32) all had a diameter of roughly 150 nm with narrow polydispersity. Two selected nanocages, **Pt(Vio)** and **Pd(Vio)** (found to be the only ones active in silencing in initial experiments, *vide infra*), were investigated in cell-uptake studies. All nanocage/siRNA assemblies were evaluated in their ability to silence GFP fluorescence in cells.

Cell-uptake studies

In the initial study, we studied the cell uptake (transfection) of two of the formed NPs, siRNA⊂**Pt(Vio)** and siRNA⊂**Pd(Vio)**. To study uptake and localization of both the cage components and the siRNA upon cell entry, we used 20% cyanine5
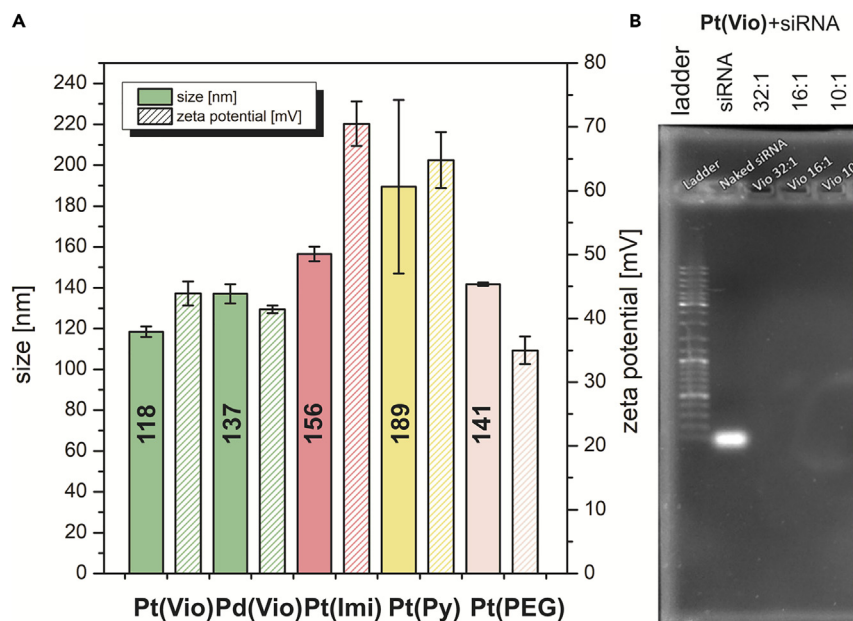
Figure 6. Characterization of nanocage-RNA NPs
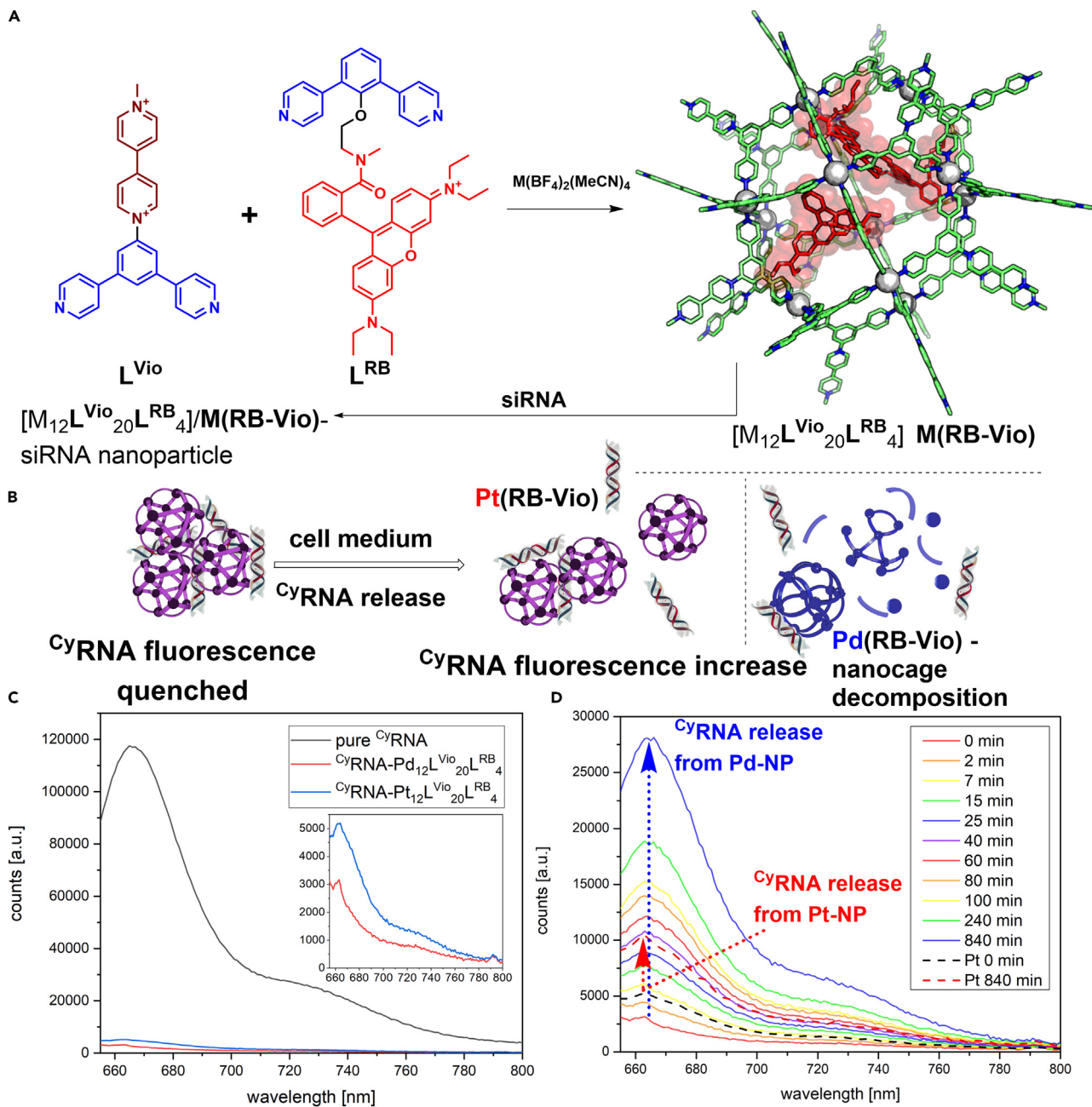
(A) Size and zeta potential for 32/1 P/N ratios of nanocage and siRNA acquired from DLS on the basis of intensity and zeta potential measurements (66 nM nanocage, 2.1 nM RNA). Error bars represent the mean ± SD; n = 3.

(B) RNA agarose gel electrophoresis of pure ^{GFP}siRNA and NPs composed of nanocage and ^{GFP}siRNA shows the disappearance of non-bound RNA (part of full gel electrophoresis image in Figure S59).

(Cy5)-labeled siRNA (^{Cy}RNA) and labeled the nanocages with rhodamine. For this, we used a mixture of 20 L^{Vio} and 4 L^{RB} building blocks during cage assembly. This afforded nanocages whose main composition [M$_{12}$L$^{Vio}_{20}$L$^{RB}_4$] (Figure 7A) had a Gaussian distribution centered around this stoichiometry of ligands, in agreement with previous results of heteroleptic nanocages.[55] The so-formed nanocages could be tracked *in vitro* and, with their high viologen content, were expected to behave similarly to the pure viologen nanocages **Pt(Vio)** and **Pd(Vio)**. We incorporated Cy5-labeled siRNA for the preparation of NPs to also track the distribution of RNA (Figures 7A and S28–S32).

Before monitoring the cellular uptake of the fluorescent RNA-nanocage NPs, we studied the properties of the NPs. When ^{Cy}RNA was incorporated into NPs (composed of RNA and **Pd(RB-Vio)** or **Pt(RB-Vio)**), the fluorescence of ^{Cy}RNA was quenched significantly (by ca. 95%; Figure 7C). The quenching of fluorescence was attributed to the successful complexation of ^{Cy}RNA with the viologen-quencher-containing nanocages. After observing the incorporation of ^{Cy}RNA into the NPs (further supported by gel electrophoresis; Figure S59) and accompanied quenching of Cy5 fluorescence, we studied both NPs in cell-growth medium (DMEM) and monitored them over time (Figure 7D). ^{Cy}RNA⊂**Pt(RB-Vio)** displayed only a little change in fluorescence over 14 h (Figure 7D), indicative of good NP stability in DMEM buffer and little RNA release (Figures 7B and 7D; further supported by ^{1}H NMR and UV-vis: Figures S63 and S64).

^{Cy}RNA⊂**Pd(RB-Vio)** showed a greater increase in the fluorescent signal of Cy5, indicating more ^{Cy}RNA release in DMEM over 14 h (Figure 7D). Because the RNA can be

Figure 7. Stability assay of cage-RNA NPs in DMEM

(A) Synthesis of rhodamine-functionalized $M_{12}L_{24}$ nanocages and the PM3-optimized structure of the nanocage.

(B) Anticipated mechanism of ^{Cy}RNA quenching by complexation with nanocages and dequenching upon release of RNA from NPs.

(C) Comparison of fluorescence of equimolar amounts of free ^{Cy}RNA and ^{Cy}RNA⊂nanocage NPs.

(D) Development of equimolar concentrations of ^{Cy}RNA⊂**Pt(RB-Vio)** and ^{Cy}RNA⊂**Pd(RB-Vio)** NPs' fluorescence over time in DMEM.

released via different mechanisms, we further studied RNA⊂Pd(**RB-Vio**) by ^{1}H NMR and UV-vis (Figures S63 and S65). As expected from the less stable palladium-based nanocage, decomposition of the nanocage into free building block L^{Vio} was observed in both UV-vis and ^{1}H NMR with comparable rates (ca. 2%–4% decomposition of nanocage per hour; Figures S63 and S65). This decomposition of the
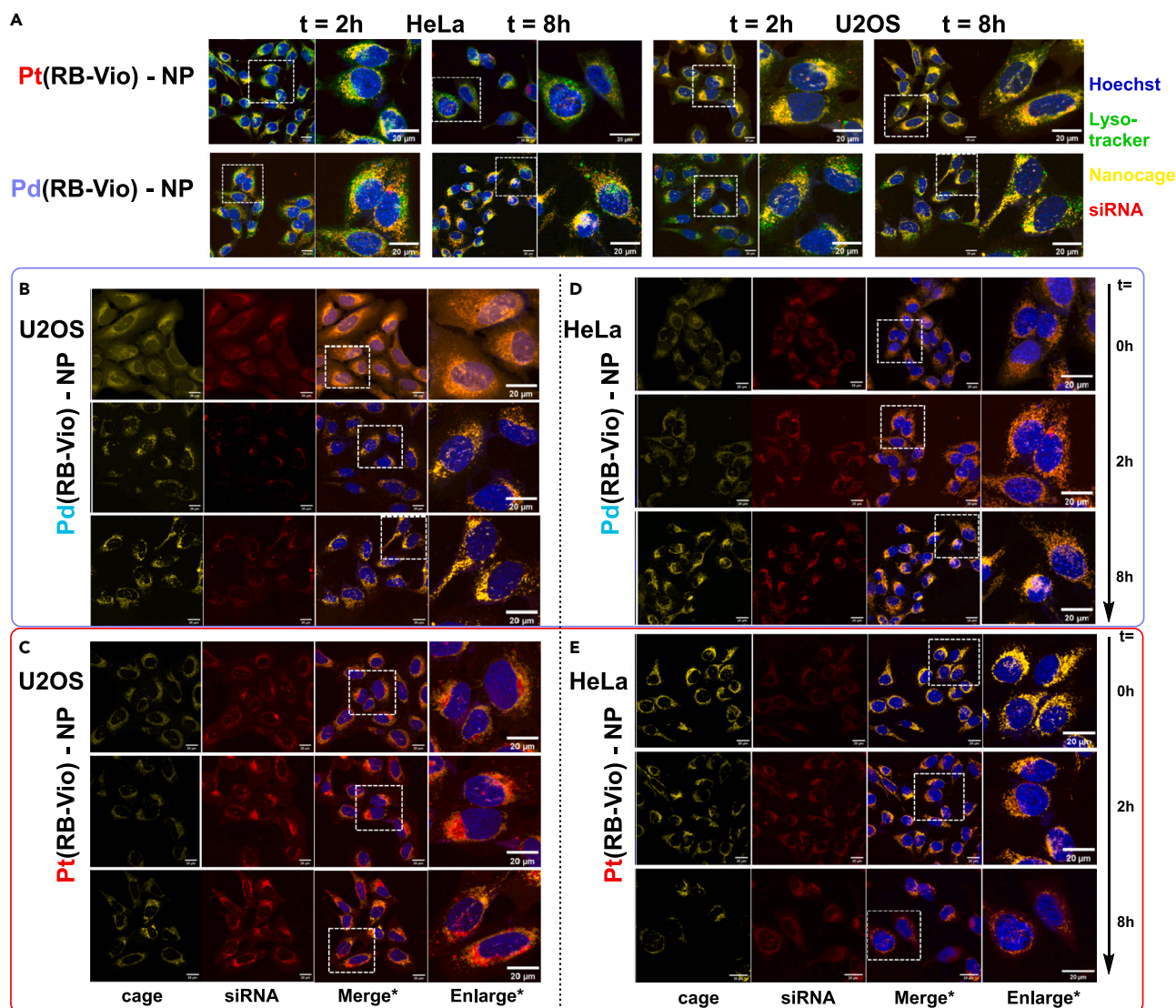
Figure 8. Cell-uptake experiments using fluorescent cage and RNA

(A) Cell uptake and development of fluorescent signal of **Pd**- and **Pt**-nanocages, RNA, and Lysotracker signal over time in U2OS and HeLa cells (2,000 ng/mL siRNA with a P/N ratio of 32/1).

(B–D) Images of cells identical to those in (A) show only the cell uptake and development of fluorescent signal of **Pd**- and **Pt**-nanocages and RNA over time in U2OS and HeLa cells (2,000 ng/mL siRNA with a P/N ratio of 32/1). *Merging and enlargement of cages, RNA, and Hoechst.

nanocage released the RNA, as supported by fluorescence (Figure 7D) and CD measurements (Figure S63). Provided that the fluorescence of ^{Cy}RNA increases upon release from NPs, this allows for direct tracking of RNA release from NPs *in vitro* (*vide infra*).

The cellular uptake was monitored by confocal imaging of the two different NPs (^{Cy}RNA⊂**Pt(RB-Vio)** and ^{Cy}RNA⊂**Pd(RB-Vio)**) on either HeLa or U2OS cells. Cells were treated for 2 h with the cage/RNA NPs and incubated for different time periods (0–8 h) before analysis by confocal microscopy (Figures 8A–8E and S67–S74).

Both ^{Cy}RNA⊂**Pt(RB-Vio)** and ^{Cy}RNA⊂**Pd(RB-Vio)** were distributed inside the cytosol of cells (Figures S68, S70, S72, and S74), and co-localization of ^{Cy}siRNA and

nanocages was observed in the cells at the incubation time (Figures 8A–8E; 0–8 h). Comparison of the cell uptake of ^{Cy}RNA⊂Pt(RB-Vio) and ^{Cy}RNA⊂Pd(RB-Vio) displayed different behaviors of the two NPs.

The ^{Cy}RNA⊂Pd(RB-Vio) NPs showed less fluorescence inside of the lysosome, whereas ^{Cy}RNA⊂Pt(RB-Vio) NPs showed more co-localization with lysosomes in HeLa. This could imply that endosomal escape is achieved more easily for ^{Cy}RNA⊂Pd(RB-Vio) NPs in HeLa cells, which could result in better siRNA delivery efficiency; however, this trend is not clear in U2OS cells.

We also observed a difference in the fluorescent signals of nanocage and ^{Cy}RNA. When comparing the Pt- and Pd-based NPs in U2OS cells, we observed a decrease in Pd(RB-Vio) and ^{Cy}RNA signal for the Pd-based system (Figure 8B). In contrast, the Pt-based NPs showed steady or increasing fluorescence for rhodamine and ^{Cy}RNA in U2OS cells. Furthermore, in various places of the cells incubated for 2 and 8 h, ^{Cy}RNA⊂Pt(RB-Vio) showed big clusters of RNA in the absence of clusters of cages (Figure 8C). This could suggest the release of the RNA from the particles. In HeLa cells, ^{Cy}RNA⊂Pd(RB-Vio) NPs displayed increased ^{Cy}RNA and nanocage signal accompanied by the formation of RNA clusters at different locations to the nanocage (Figure 8D). Conversely, ^{Cy}RNA⊂Pt(RB-Vio) showed decreased nanocage and ^{Cy}RNA signal and after only 8 h showed an indication of RNA release (Figure 8E).

Whereas the cell-specific behavior (Pd-NP RNA release in HeLa cells and Pt-NP RNA release in U2OS cells) can be the result of different factors (such as local pH or enzymatic and molecular content of the different cell lines), it has an influence on gene expression and is to the best of our knowledge a unique feature of nanocages derived from the same building block and differing only in the metal nodes.

Silencing efficiency of NPs after ^{GFP}siRNA delivery

For siRNA delivery, a potent silencing effect of target genes represents effective siRNA delivery vectors. Therefore, we investigated the intracellular ^{GFP}siRNA delivery efficiency of NPs. GFP is a reporter protein of 238 amino acids and emits a bright green fluorescence (λ_{max} = 509 nm) when illuminated with a blue light (λ_{max} = 490 nm), and it has been widely used to detect gene expression because its fluorescence directly reflects the levels of gene expression.[62,63] Intracellular ^{GFP}siRNA induces gene silencing by targeting complementary mRNA for degradation, leading to a decrease in GFP fluorescence (Figure 9A). To do this, we used two GFP-expressing cell lines, HeLa-CD63-GFP and U2OS-UBE231-GFP, for the easy detection of ^{GFP}siRNA delivery efficiency by quantifying the GFP fluorescence differences of cells.[64,65] NPs loaded with ^{GFP}siRNA were incubated with cells for 24 h, after which the growth medium was changed, the NPs were incubated for 24 h (Figure 9B; for 48 h, see Figure S79) at different siRNA concentrations, and the fluorescence of cells was quantified by flow cytometry (Figure 9C). The commercial transfection reagent lipofectamine 3K was used as a positive control. Given that GFP is also silenced when cell death is occurring, we detected the GFP mean fluorescence intensity (MFI) by gating (selecting) only the live cells for our quantification and analysis. This way, GFP silencing efficiency was not correlated to the toxicity of a vector (vide infra). Moreover, we performed control experiments with non-active RNA and nanocages to fully exclude the correlation between toxicity and GFP silencing.
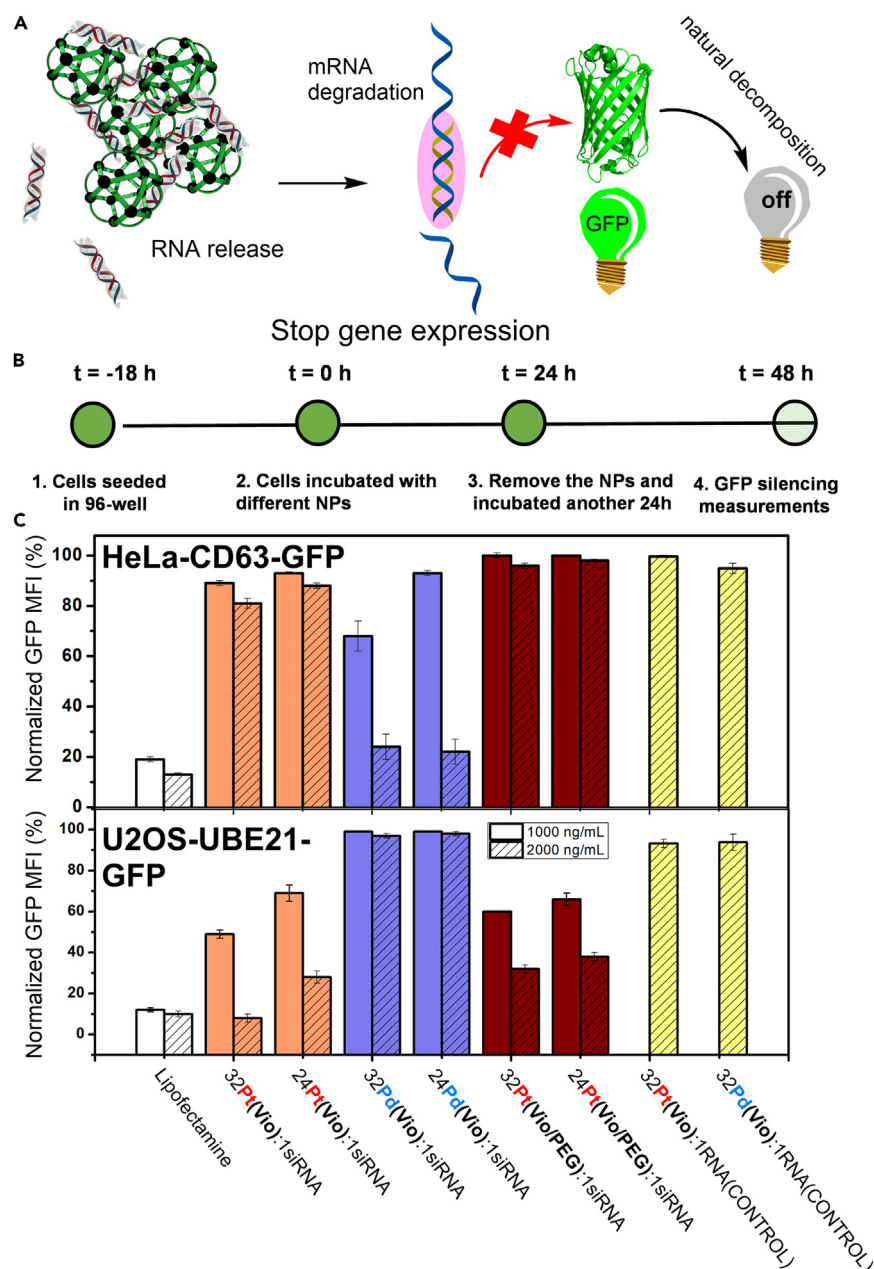
Figure 9. Transfection efficiency of nanocage-RNA NPs

(A) Schematic description of the experimental setup.

(B) Timeline of experimental expression efficiency assay.

(C) Normalized GFP MFI of HeLa-CD63-GFP and U2OS-UBE21-GFP cells after incubation of different nanocage-RNA NPs encapsulating ^{GFP}siRNA and non-sense siRNA (normalized against untreated cells). Error bars represent the mean ± SD. n = 3.

Among all nanocage-based NPs, ^{GFP}siRNA⊂Pd(Vio) exhibited the highest silencing potency on the HeLa cell line. It reduced the GFP expression by 76% when 32/1 (P/N) of ^{GFP}siRNA⊂Pd(Vio) was used. Interestingly, the same ^{GFP}siRNA⊂Pd(Vio) NP showed no silencing effect at all on the U2OS cell line (Figure 9C).

^{GFP}siRNA⊂Pt(Vio) showed a lower silencing potency in HeLa cells with a 19% reduction in GFP expression. However, ^{GFP}siRNA⊂Pt(Vio) showed the highest silencing

potency in the U2OS cell line with over 90% GFP reduction, which is comparable to the silencing potency of lipofectamine (Figure 9C).

Importantly, whereas the NPs formed from different nanocages differentiated between the two cell lines in a single cell-line experiment with high GFP silencing selectivity (66% U2OS selectivity for ^{GFP}siRNA⊂Pt(Vio); 92% HeLa selectivity for ^{GFP}siRNA⊂Pd(Vio)), the commercial transfection agent lipofectamine displayed significantly lower selectivity (ca. 2% U2OS selectivity over HeLa cells; Figure 9C). Importantly, GFP silencing was not observed when an inactive RNA sequence was applied (^{CONTROL}RNA⊂Pt(Vio) or ^{CONTROL}RNA⊂Pd(Vio); Figure 9C), ruling out selectivity and activity derived from potential toxicity of the nanocages.

Because we anticipated that the viologen-containing nanocage vectors could exhibit toxicity (vide infra), we also investigated a mixed nanocage containing 50% L^{Vio} and 50% of the less harmful L^{PEG} in the silencing experiment (^{GFP}siRNA⊂Pt(Vio-PEG); see supplemental information section "cage stability studies"). Indeed, the mixed nanocage Pt(Vio-PEG) exhibited GFP silencing efficiencies in analogy to pure Pt(Vio), i.e., both vectors showed silencing selectivity for U2OS cells. In comparison to Pt(Vio), the mixed nanocage Pt(Vio-PEG) showed lower silencing efficiency on both cell lines (e.g., in U2OS, 68% for Pt(Vio-PEG) and 92% using Pt(Vio)) and no detectable silencing in HeLa cells. In combination with evaluating cellular uptake, we suspected that this different cell-selective silencing effect after siRNA delivery resulted from different RNA releases of NPs inside different cell lines.

Cytotoxicity of NPs and discussion

After the successful siRNA delivery, which was observed with Pt(Vio), Pt(Vio-PEG), and Pd(Vio) as vectors, the toxicity of the formed NPs was briefly investigated on the two cell lines. The cell viability was evaluated after 24 h of RNA⊂nanocage treatment and 24 h (for 48 h, see Figure S76) of incubation (in the same time frame as the GFP silencing experiments; Figure 10A). siRNA⊂Pd(Vio) showed higher cytotoxicity to HeLa cells (64%) than to U2OS cells (14%). In contrast, siRNA⊂Pt(Vio) showed lower toxicity against HeLa (25%) and higher toxicity against U2OS (35%). Interestingly, the mixed nanocage NP siRNA⊂Pt(Vio/PEG) displayed less cytotoxicity than the pure viologen NP (siRNA⊂Pt(Vio)) (4% for HeLa and 28% for U2OS).

The toxicity of siRNA⊂Pd(Vio) was selective for HeLa (64%) over U2OS (15%), and so was the GFP silencing (76% for HeLa and 3% for U2OS). Similar trends also applied to the platinum-based NPs, i.e., both were more toxic against U2OS and display more silencing in U2OS. Because NPs that show little GFP silencing also display little toxicity (e.g., siRNA⊂Pd(Vio) showed little toxicity and silencing for U2OS), we anticipate that the NPs made from nanocages and RNA are a little toxic (Figure 10B, left). We hypothesize that upon the release of siRNA (and consecutive GFP silencing), free nanocages are released, which is cytotoxic (Figure 10B, right).[66,67]

Depending on the envisioned application (research, gene therapy, or cancer treatment), the toxicity of the free nanocages (released from NPs after RNA release) has to be tuned further. As such, we envision that toxic NPs (such as RNA⊂Pd(Vio) for HeLa cells) could be suitable for cancer treatment in which the nanocage and the RNA can be dual cytotoxic to tumor cells after the loading of an anti-tumor siRNA. For other gene therapeutic applications, the toxicity of the nanocages (vectors) has to be lowered. We show that this can be partially achieved with the more robust platinum nanocages or mixtures of building blocks for nanocage assembly.
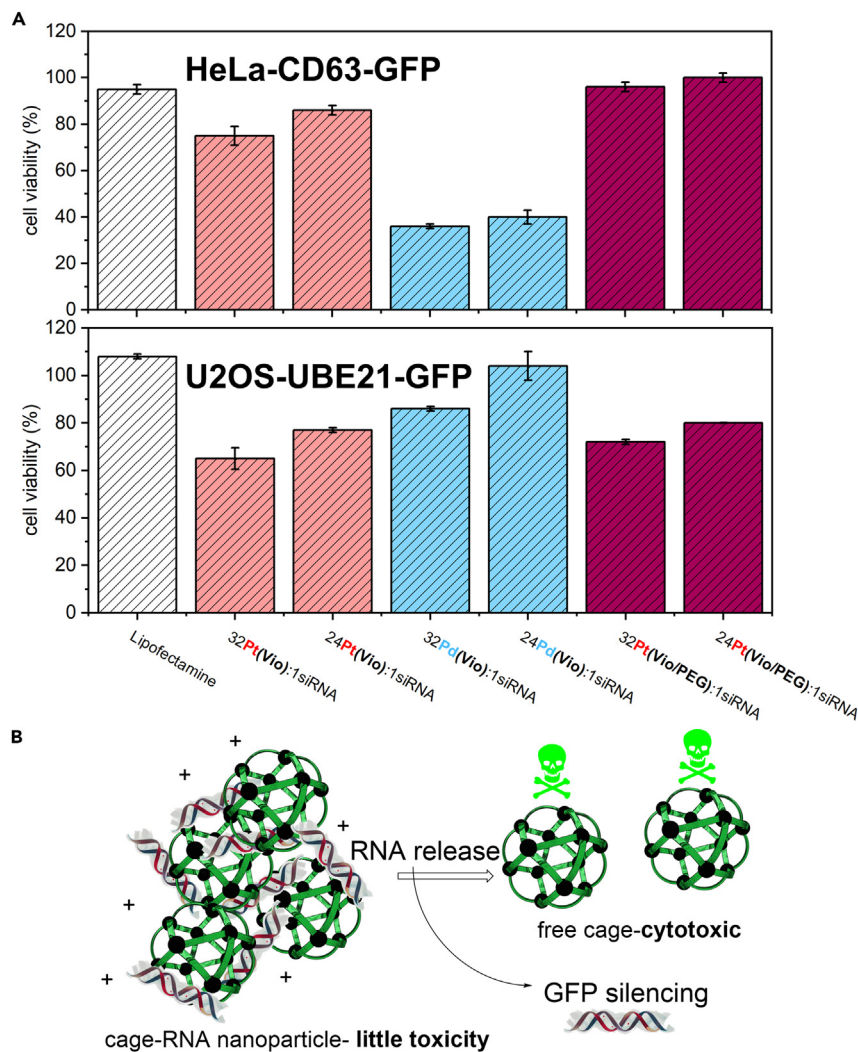
Figure 10. Cell-viability evaluation of different NPs on HeLa-CD63-GFP and U2OS-UBE21-GFP cells

(A) Cell viability ($\pm$SD) after 24 h of treatment of different cell lines with 2,000 ng/mL ^{GFP}siRNA and different ratios of nanocages. Error bars represent the mean $\pm$ SD. n = 3.

(B) Anticipated origin of toxicity.

However, obtaining an even more harmless system for therapeutic gene delivery would require further modification.

Certainly, the realization of therapeutic applications requires more studies, including *in vivo* studies, given that the *in vitro* experiments shown in this work represent a highly controlled simplified version of complex living matter. Nevertheless, this pioneering study shows that nanocages are capable of binding and releasing RNA *in vitro*, and these are promising features for further research.

Conclusion

In summary, we have reported the design and synthesis of five different $M_{12}L_{24}$ cages that are able to form RNA$\subset M_{12}L_{24}$ NPs. Simple monomeric building blocks, exteriorly functionalized with different binding sites for nucleic acids, have been

prepared. When combined with platinum or palladium, this selectively yields the corresponding $M_{12}L_{24}$ nanocages. Whereas platinum-based cages have good stability against many typically found biological components, the palladium analogs decompose under identical conditions. All cages complex siRNA efficiently and form nanosized (110–190 nm) RNA⊂$M_{12}L_{24}$ NPs with highly cationic zeta potential depending on the nanocage composition. The so-formed NPs show metal-dependent accumulation and release of siRNA in two different cell lines. Whereas HeLa cells show long-term accumulation and release of RNA *in vitro* with RNA⊂**Pd(Vio)**, U2OS cell lines show cell-specific (among these two cell lines) accumulation and release of RNA with RNA⊂**Pt(Vio)**. In line with these observations, HeLa cells and U2OS cells show highly selective gene expression of an implemented ^{GFP}siRNA with RNA⊂**Pd(Vio)** and RNA⊂**Pt(Vio)**, respectively. This unique cell-selectivity feature of the NPs (in contrast to lipofectamine, which exhibits no selectivity) in siRNA delivery offers a promising addition to the field of targeted RNA gene-material delivery, and its full potential has yet to be uncovered. Although only highly controlled *in vitro* results of RNA delivery of nanocage vectors have been performed so far, we have shown that nanocages are suitable vectors for cell-specific RNA delivery through simple variation of the sphere-forming metal nodes. This provides a tunability handle for future developments into highly desirable selective RNA nanomedicines.

EXPERIMENTAL PROCEDURES

Resource availability

Lead contact
Further information and requests for resources should be directed to the lead contact, Joost N.H. Reek (j.n.h.reek@uva.nl).

Materials availability
This study did not generate new unique reagents.

Data and code availability
All data are available from the corresponding author upon reasonable request. No codes were developed.

SUPPLEMENTAL INFORMATION

Supplemental information can be found online at https://doi.org/10.1016/j.chempr.2023.03.018.

ACKNOWLEDGMENTS

AUTHOR CONTRIBUTIONS

E.O.B. and Y.Z. (in alphabetic order) contributed equally to this work. Conceptualization, E.O.B., Y.Z., A.K., and J.N.H.R.; formal analysis, E.O.B. and Y.Z.; funding acquisition, J.N.H.R., B.d.B., and A.K.; investigation, E.O.B., Y.Z., K.W., E.K., and E.M.M.; supervision, J.N.H.R. and A.K.; validation, E.O.B., Y.Z., K.W., E.K., E.M.M., B.d.B., A.K., and J.N.H.R.; visualization, E.O.B.; writing – original draft, E.O.B.; writing – review & editing, E.O.B., Y.Z., K.W., E.K., B.d.B., A.K., and J.N.H.R.

REFERENCES

1. Mendes, B.B., Conniot, J., Avital, A., Yao, D., Jiang, X., Zhou, X., Sharf-Pauker, N., Xiao, Y., Adir, O., Liang, H., et al. (2022). Nanodelivery of nucleic acids. Nat. Rev. Methods Primers 2, 24.

2. Alimi, L.O., Alyami, M.Z., Chand, S., Baslyman, W., and Khashab, N.M. (2021). Coordination-based self-assembled capsules (SACs) for protein, CRISPR–Cas9, DNA and RNA delivery. Chem. Sci. 12, 2329–2344.

3. Fang, H., Feng, Y., Chen, J., Tian, H., and Chen, X. (2019). Constructing efficient polycationic gene carriers through regulating the physicochemical properties. Mater. Today Chem. 11, 269–282.

4. Mingozzi, F., and High, K.A. (2011). Therapeutic in vivo gene transfer for genetic disease using AAV: progress and challenges. Nat. Rev. Genet. 12, 341–355.

5. Bush, A., Alton, E.W.F.W., Davies, J.C., Griesenbach, U., and Jaffe, A. (2005). In Cystic Fibrosis in the 21st Century (S. Karger AG). https://doi.org/10.1159/isbn.978-3-318-01240-8.

6. Cheng, C.J., Bahal, R., Babar, I.A., Pincus, Z., Barrera, F., Liu, C., Svoronos, A., Braddock, D.T., Glazer, P.M., Engelman, D.M., et al. (2015). MicroRNA silencing for cancer therapy targeted to the tumour microenvironment. Nature 518, 107–110.

7. Park, J., Singha, K., Son, S., Kim, J., Namgung, R., Yun, C.O., and Kim, W.J. (2012). A review of RGD-functionalized nonviral gene delivery vectors for cancer therapy. Cancer Gene Ther. 19, 741–748.

8. Izquierdo, M. (2005). Short interfering RNAs as a tool for cancer gene therapy. Cancer Gene Ther. 12, 217–227.

9. Roth, G.A., Mensah, G.A., Johnson, C.O., Addolorato, G., Ammirati, E., Baddour, L.M., Barengo, N.C., Beaton, A.Z., Benjamin, E.J., Benziger, C.P., et al. (2020). Global burden of cardiovascular diseases and risk factors, 1990–2019. J. Am. Coll. Cardiol. 76, 2982–3021.

10. Frank, T.D., Carter, A., Jahagirdar, D., Biehl, M.H., Douwes-Schultz, D., Larson, S.L., Arora, M., Dwyer-Lindgren, L., Steuben, K.M., and Abbastabar, H. (2019). Global, regional, and national incidence, prevalence, and mortality of HIV, 1980–2017, and forecasts to 2030, for 195 countries and territories: a systematic analysis for the Global Burden of Diseases, Injuries, and Risk Factors Study 2017. Lancet HIV 6, e831–e859.

11. Adli, M. (2018). The CRISPR tool kit for genome editing and beyond. Nat. Commun. 9, 1911.

12. Anzalone, A.V., Koblan, L.W., and Liu, D.R. (2020). Genome editing with CRISPR–Cas nucleases, base editors, transposases and prime editors. Nat. Biotechnol. 38, 824–844.

13. Agrawal, N., Dasaradhi, P.V.N., Mohmmed, A., Malhotra, P., Bhatnagar, R.K., and Mukherjee, S.K. (2003). RNA interference: biology, mechanism, and applications. Microbiol. Mol. Biol. Rev. 67, 657–685.

14. Wilson, R.C., and Doudna, J.A. (2013). Molecular mechanisms of RNA interference. Annu. Rev. Biophys. 42, 217–239.

15. Setten, R.L., Rossi, J.J., and Han, S.P. (2019). The current state and future directions of RNAi-based therapeutics. Nat. Rev. Drug Discov. 18, 421–446.

16. Akinc, A., Querbes, W., De, S., Qin, J., Frank-Kamenetsky, M., Jayaprakash, K.N., Jayaraman, M., Rajeev, K.G., Cantley, W.L., Dorkin, J.R., et al. (2010). Targeted delivery of RNAi therapeutics with endogenous and exogenous ligand-based mechanisms. Mol. Ther. 18, 1357–1364.

17. Soutschek, J., Akinc, A., Bramlage, B., Charisse, K., Constien, R., Donoghue, M., Elbashir, S., Geick, A., Hadwiger, P., Harborth, J., et al. (2004). Therapeutic silencing of an endogenous gene by systemic administration of modified siRNAs. Nature 432, 173–178.

18. Rietwyk, S., and Peer, D. (2017). Next-generation lipids in RNA interference therapeutics. ACS Nano 11, 7572–7586.

19. Hoy, S.M. (2018). Patisiran: first global approval. Drugs 78, 1625–1631.

20. Bulaklak, K., and Gersbach, C.A. (2020). The once and future gene therapy. Nat. Commun. 11, 5820.

21. Shahryari, A., Burtscher, I., Nazari, Z., and Lickert, H. (2021). Engineering gene therapy: advances and barriers. Adv. Therap. 4, 2100040.

22. Papanikolaou, E., and Bosio, A. (2021). The promise and the hope of gene therapy. Front Genome Ed. 3, 618346.

23. Al-Dosari, M.S., and Gao, X. (2009). Nonviral gene delivery: principle, limitations, and recent progress. AAPS J. 11, 671–681.

24. Bono, N., Ponti, F., Mantovani, D., and Candiani, G. (2020). Non-viral in vitro gene delivery: it is now time to set the bar! Pharmaceutics 12, 183.

25. Gao, X., Kim, K.S., and Liu, D. (2007). Nonviral gene delivery: what we know and what is next. AAPS J. 9, E92–E104.

26. Nayak, S., and Herzog, R.W. (2010). Progress and prospects: immune responses to viral vectors. Gene Ther. 17, 295–304.

27. Yu, T., Liu, X., Bolcato-Bellemin, A.L., Wang, Y., Liu, C., Erbacher, P., Qu, F., Rocchi, P., Behr, J.P., and Peng, L. (2012). An amphiphilic dendrimer for effective delivery of small interfering RNA and gene silencing in vitro and in vivo. Angew. Chem. Int. Ed. 51, 8478–8484.

28. Kesharwani, P., and Iyer, A.K. (2015). Recent advances in dendrimer-based nanovectors for tumor-targeted drug and gene delivery. Drug Discov. Today 20, 536–547.

29. Zhao, Y., and Huang, L. (2014). Lipid nanoparticles for gene delivery. In Nonviral Vectors for Gene Therapy – Lipid- and Polymer-Based Gene Transfer (Academic Press), pp. 13–36.

30. del Pozo-Rodríguez, A., Solinís, M.Á., and Rodríguez-Gascón, A. (2016). Applications of lipid nanoparticles in gene therapy. Eur. J. Pharm. Biopharm. 109, 184–193.

31. Liu, Y., Liggitt, D., Zhong, W., Tu, G., Gaensler, K., and Debs, R. (1995). Cationic liposome-mediated intravenous gene delivery. J. Biol. Chem. 270, 24864–24870.

32. Templeton, N.S. (2002). Cationic liposome-mediated gene delivery in vivo. Biosci. Rep. 22, 283–295.

33. Poddar, A., Conesa, J.J., Liang, K., Dhakal, S., Reineck, P., Bryant, G., Pereiro, E., Ricco, R., Amenitsch, H., Doonan, C., et al. (2019). Encapsulation, visualization and expression of genes with biomimetically mineralized zeolitic imidazolate framework-8 (ZIF-8). Small 15, e1902268.

34. Yu, K., Wei, T., Li, Z., Li, J., Wang, Z., and Dai, Z. (2020). Construction of molecular sensing and logic systems based on site-occupying effect-modulated MOF–DNA interaction. J. Am. Chem. Soc. 142, 21267–21271.

35. Alsaiari, S.K., Patil, S., Alyami, M., Alamoudi, K.O., Aleisa, F.A., Merzaban, J.S., Li, M., and Khashab, N.M. (2018). Endosomal escape and delivery of CRISPR/Cas9 genome editing machinery enabled by nanoscale zeolitic imidazolate framework. J. Am. Chem. Soc. 140, 143–146.

36. Wang, C., Di, Z., Xiang, Z., Zhao, J., and Li, L. (2021). Coordination-driven assembly of proteins and nucleic acids in a single architecture for carrier-free intracellular co-delivery. Nano Today 38, 101140.

37. Yue, Y., and Wu, C. (2013). Progress and perspectives in developing polymeric vectors

for in vitro gene delivery. Biomater. Sci. *1*, 152–170.

38. Green, J.J., Shi, J., Chiu, E., Leshchiner, E.S., Langer, R., and Anderson, D.G. (2006). Biodegradable polymeric vectors for gene delivery to human endothelial cells. Bioconjug. Chem. *17*, 1162–1169.

39. Li, S., and Huang, L. (2000). Nonviral gene therapy: promises and challenges. Gene Ther. *7*, 31–34.

40. Das, S.K., Menezes, M.E., Bhatia, S., Wang, X.Y., Emdad, L., Sarkar, D., and Fisher, P.B. (2015). Gene therapies for cancer: strategies, challenges and successes. J. Cell. Physiol. *230*, 259–271.

41. Pöthig, A., and Casini, A. (2019). Recent developments of supramolecular metal-based structures for applications in cancer therapy and imaging. Theranostics 9, 3150–3169.

42. Sun, Y., Chen, C., Liu, J., and Stang, P.J. (2020). Recent developments in the construction and applications of platinum-based metallacycles and metallacages via coordination. Chem. Soc. Rev. *49*, 3889–3919.

43. Lu, Z., Bai, S., Shi, Y., Xu, D., Chu, C., and Liu, G. (2021). Artificial nanocage-based 3D framework platforms: from construction design to biomedical applications. Chem. Eng. J. *426*, 131891.

44. Kumar, S., Jana, A., Bhowmick, S., and Das, N. (2022). Topical progress in medicinal applications of self-assembled organoplatinum complexes using diverse Pt(II)- and N-based tectons. Appl. Organomet. Chem. *36*, e6722.

45. Chakrabarty, R., Mukherjee, P.S., and Stang, P.J. (2011). Supramolecular coordination: self-assembly of finite two- and three-dimensional ensembles. Chem. Rev. *111*, 6810–6918.

46. Harris, K., Fujita, D., and Fujita, M. (2013). Giant hollow M_nL_{2n} spherical complexes: structure, functionalisation and applications. Chem. Commun. *49*, 6703–6712.

47. Pullen, S., Tessarolo, J., and Clever, G.H. (2021). Increasing structural and functional complexity in self-assembled coordination cages. Chem. Sci. *12*, 7269–7293.

48. Zhang, D., Ronson, T.K., and Nitschke, J.R. (2018). Functional capsules via subcomponent self-assembly. Acc. Chem. Res. *51*, 2423–2436.

49. Vajpayee, V., Yang, Y.J., Kang, S.C., Kim, H., Kim, I.S., Wang, M., Stang, P.J., and Chi, K.W. (2011). Hexanuclear self-assembled arene-ruthenium nano-prismatic cages: potential anticancer agents. Chem. Commun. *47*, 5184–5186.

50. Zheng, Y.R., Suntharalingam, K., Bruno, P.M., Lin, W., Wang, W., Hemann, M.T., and Lippard, S.J. (2016). Mechanistic studies of the anticancer activity of an octahedral hexanuclear Pt(II) cage. Inorganica. Chim. Acta *452*, 125–129.

51. Xi, S.F., Bao, L.Y., Lin, J.G., Liu, Q.Z., Qiu, L., Zhang, F.L., Wang, Y.X., Ding, Z.D., Li, K., and Gu, Z.G. (2016). Enantiomers of tetrahedral metal–organic cages: a new class of highly efficient G-quadruplex ligands with potential anticancer activities. Chem. Commun. *52*, 10261–10264.

52. Xu, X.X., Na, J.J., Bao, F.F., Zhou, W., Pang, C.Y., Li, Z., and Gu, Z.G. (2014). Dinuclear nickel(II) triple-stranded supramolecular cylinders: syntheses, characterization and G-quadruplexes binding properties. Spectrochim. Acta A Mol. Biomol. Spectrosc. *124*, 21–29.

53. Kikuchi, T., Sato, S., Fujita, D., and Fujita, M. (2014). Stepwise DNA condensation by a histone-mimic peptide-coated $M_{12}L_{24}$ spherical complex. Chem. Sci. *5*, 3257.

54. Sato, S., Ishido, Y., and Fujita, M. (2009). Remarkable stabilization of $M_{12}L_{24}$ spherical frameworks through the cooperation of 48 Pd(II)-pyridine interactions. J. Am. Chem. Soc. *131*, 6064–6065.

55. Bobylev, E.O., Poole, D.A., III, de Bruin, B., and Reek, J.N.H. (2021). How to prepare kinetically stable self-assembled $Pt_{12}L_{24}$ nanocages while circumventing kinetic traps. Chem. Eur. J. *27*, 12667–12674.

56. Yan, X., Wei, P., Liu, Y., Wang, M., Chen, C., Zhao, J., Li, G., Saha, M.L., Zhou, Z., An, Z., et al. (2019). Endo- and Exo-Functionalized tetraphenylethylene $M_{12}L_{24}$ nanospheres: fluorescence emission inside a confined space. J. Am. Chem. Soc. *141*, 9673–9679.

57. Bobylev, E.O., Poole, D.A., III, de Bruin, B., and Reek, J.N.H. (2021). Selective formation of $Pt_{12}L_{24}$ nanospheres by ligand design. Chem. Sci. *12*, 7696–7705.

58. Fujita, D., Suzuki, K., Sato, S., Yagi-Utsumi, M., Yamaguchi, Y., Mizuno, N., Kumasaka, T., Takata, M., Noda, M., Uchiyama, S., et al. (2012). Protein encapsulation within synthetic molecular hosts. Nat. Commun. *3*, 1093.

59. Supramolecular.org. BindFit v.0.5. http://supramolecular.org.

60. Thordarson, P. (2011). Determining association constants from titration experiments in supramolecular chemistry. Chem. Soc. Rev. *40*, 1305–1323.

61. Brynn Hibbert, D., and Thordarson, P. (2016). The death of the Job plot, transparency, open science and online tools, uncertainty estimation methods and other developments in supramolecular chemistry data analysis. Chem. Commun. *52*, 12792–12805.

62. Chalfie, M., Tu, Y., Euskirchen, G., Ward, W.W., and Prasher, D.C. (1994). Green fluorescent protein as a marker for gene expression. Science *263*, 802–805.

63. Kar-Roy, A., Dong, W., Michael, N., and Li, Y. (2000). Green fluorescence protein as a transcriptional reporter for the long terminal repeats of the human immunodeficiency virus type 1. J. Virol. Methods *84*, 127–138.

64. Jongsma, M.L.M., Berlin, I., Wijdeven, R.H.M., Janssen, L., Janssen, G.M.C., Garstka, M.A., Janssen, H., Mensink, M., van Veelen, P.A., Spaapen, R.M., and Neefjes, J. (2016). An ER-associated pathway defines endosomal architecture for controlled cargo transport. Cell *166*, 152–166.

65. Qiao, X., van der Zanden, S.Y., Wander, D.P.A., Borràs, D.M., Song, J.Y., Li, X., van Duikeren, S., van Gils, N., Rutten, A., van Herwaarden, T., et al. (2020). Uncoupling DNA damage from chromatin damage to detoxify doxorubicin. Proc. Natl. Acad. Sci. USA *117*, 15182–15192.

66. Samanta, S.K., Moncelet, D., Briken, V., and Isaacs, L. (2016). Metal–organic polyhedron capped with Cucurbit[8]uril delivers doxorubicin to cancer cells. J. Am. Chem. Soc. *138*, 14488–14496.

67. Lazarević, T., Rilak, A., and Bugarčić, Ž.D. (2017). Platinum, palladium, gold and ruthenium complexes as anticancer agents: current clinical uses, cytotoxicity studies and future perspectives. Eur. J. Med. Chem. *142*, 8–31.